ACS Catalysis

pubs.acs.org/acscatalysis Letter

Coadsorption of NRR and HER Intermediates Determines the Performance of Ru-N_4 toward Electrocatalytic N_2 Reduction

Tongwei Wu, Marko M. Melander, and Karoliina Honkala*

Cite This: *ACS Catal.* 2022, 12, 2505−2512 Read Online

ACCESS | Metrics & More | Article Recommendations | Supporting Information

ABSTRACT: Electrochemical N_2 reduction (NRR) to ammonia is seriously limited by the competing hydrogen evolution reaction (HER), but atomic-scale factors controlling HER/NRR competition are unknown. Herein we unveil the mechanism, thermodynamics, and kinetics determining the HER/NRR efficiency on the state-of-the-art NRR electrocatalyst, Ru-N_4, using grand canonical ensemble density functional theory (GCE-DFT). We show that NRR/HER intermediates coadsorb on the catalyst where NRR intermediates suppress HER and selectivity is determined by the initial step forming *NNH or *H. Our results provide crucial insight into the complex NRR/HER competition, show the necessity of using GCE-DFT calculations, and suggest ways to improve NRR selectivity.

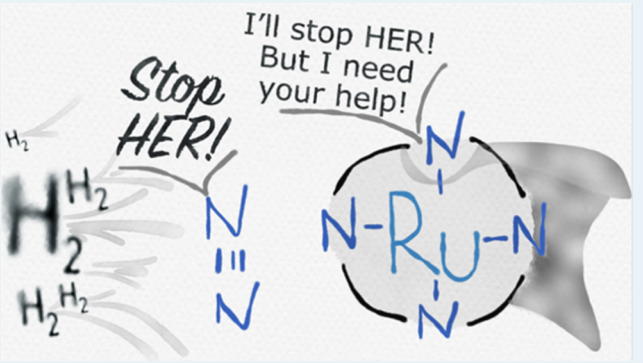

KEYWORDS: *hydrogen evolution reaction, electrochemical N_2 reduction, grand canonical ensemble density functional theory*

Ammonia is one of the most important chemicals in modern industries and agriculture. The Haber−Bosch process was developed to industrially reduce N_2 to NH_3 in the early 1900s.[1−4] This process, however, has a large carbon footprint, causing 1−2% of the world's annual energy consumption and CO_2 emissions.[5−7] The high environmental cost is in large part due to the production of pure hydrogen through methane steam-reforming at high reaction temperatures and pressures. Electrochemical N_2 reduction reaction (NRR) in aqueous electrolytes emerges as an attractive environmentally friendly alternative for sustainable ammonia production.[6,7] Nevertheless, the NRR is seriously limited by the strong N≡N bond, low solubility of N_2 in water, slow reaction kinetics, and the competing hydrogen evolution reaction (HER).[6−9]

Presently, various strategies such as catalyst design, electrolyte modulation, and reactor optimization[6−17] are being investigated as means to improve NRR activity and to limit the HER in aqueous electrolytes. Although the most significant improvements in NRR performance have been achieved through the electrocatalyst design approach,[8] it is hindered by simultaneously requiring strong N_2 adsorption and limited HER activity.[18−22] Often, catalyst design is based on thermodynamic principles but scaling relations between HER and NRR intermediates indicate that HER cannot be satisfactorily suppressed through thermodynamic control alone.[21−26] Alternative design principles aim to optimize NRR through controlling reaction kinetics but this is also difficult since free-energy scaling relations indicate that the NRR is kinetically slower than the HER.[26−29]

In addition to improving the electrocatalytic materials, modulation of the reaction environment through electrolyte design and limiting hydrogen transport to the active site has also been recognized as an efficient strategy to selectively facilitate NRR.[9,22] A recent experimental study on the role of different electrolyte counterions (Li^+, Na^+, and K^+) showed that the interaction between Li^+ and N_2 molecules can markedly enhance N_2 concentration at the electrode surface.[10] It has also been shown that regulation of proton and nitrogen diffusion combined with cation-dependent stabilization of NRR intermediates can be leveraged to reach higher activity and selectivity for NRR.[23] Recently, this strategy of combining electrolyte design with controlled hydrogen transport through "molecular crowding" was identified as an efficient approach to suppress HER and enhance NRR.[16]

Despite significant advances in improving electrocatalytic materials, electrolyte composition, and transport properties, the competing HER still limits overall NRR performance,[8,10,25−29] and low selectivity, current density, and energy efficiency of present electrocatalytic systems make NRR unviable at the industrial scale.[30] Current state-of-the-art catalysts are still far away from the performance of ideal

Received: December 17, 2021
Revised: January 27, 2022

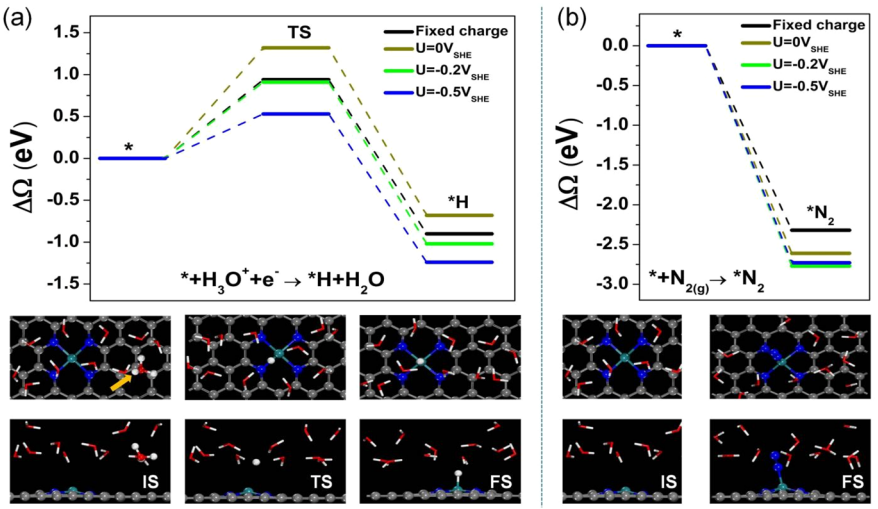

Figure 1. (a) The Volmer reaction ($H_3O^+ + e^- \rightarrow *H + H_2O$) and (b) the N_2 adsorption on bare Ru-N_4 site. In (a), IS, TS, and FS represent initial, transition, and final states of the Volmer reaction, respectively. In (b), IS corresponds to N_2(g) and FS to $*N_2$.

catalysts or that of naturally occurring nitrogenaze enzymes, which catalyze the N_2 to NH_3 reaction with high activity and selectivity under mild reaction conditions.[30] The near-ideal performance of nitrogenases[30] can be attributed to the combination of an active NRR catalytic site and the limited number of protons near this site.[25,31,32] This implies that in addition to the NRR catalytically active site, the reaction environment has a central role in NRR (electro)catalysis. Transferring this inspiration to catalyst design requires a better understanding of the factors controlling HER/NRR competition at the atomic level.[30]

It is well-known that the competing NRR and HER reaction steps may take place on a single common active site or on two separate sites,[33,34] where the former offers a more well-defined reaction environment. In contrast, extended surfaces are nonuniform and have multiple active sites for competing reactions which often limits the achievable selectivity unless some very advanced catalyst architechures are employed.[15] In general, single-[35] or biatom nanocatalysts[36] (SACs and BACs, respectively) provide a more restricted reaction environment as the presence of a single or few metal active centers confine NRR and HER to the same or nearby sites. Therefore, SACs and BACs are among the best catalysts to address the competition between NRR and HER.[35−38] In particular, various SACs, such as transition metals/g-C_3N_4, Mo-BN, single-boron, Mo(Cr)/N_3-G, and Ru-N_4-G,[17,18,39−43] have proven to be efficient for NRR. Among the different SACs, the Ru single-atom anchored on nitrogen-doped graphene (Ru-N_4) exhibits the highest experimentally verified NRR performance to date with 30% selectivity toward NRR at −0.2 V_{RHE}.[40] Despite the experimentally proven performance, the factors making Ru-N_4 such a promising catalyst remain unknown, which limits the systematic development of SACs or other electrocatalysts for NRR.

Herein, we unveil the HER/NRR competition in the Ru-N_4 using state-of-the-art constant potential, grand canonical ensemble density functional theory (GCE-DFT) simulations[44−46] using a hybrid explicit/implicit solvation treatment as detailed in the Supporting Information section S1. This advanced computational approach allows us to consider both thermodynamic and kinetic factors for competing NRR and HER pathways as a function of the electrode potential while properly accounting for solvent interactions. We observed that a GCE-DFT treatment is crucial for correctly capturing the reaction and transition state energies activity and that canonical constant-charge DFT calculations cannot even qualitatively explain the selectivity of Ru-N_4 toward NRR. Our results show that the interaction between coadsorbed hydrogen and NRR intermediates determines the NRR/HER selectivity on the Ru-N_4 catalyst. Specifically, we found the first proton-coupled electron transfer (PCET) step in NRR to control the selectivity indicating that research efforts should therefore focus on facilitating this step.

We modeled the Ru-N_x SAC as a Ru atom coordinated to four nitrogens in a porphyrin-like geometry, Ru-N_4. This model for the active site was chosen on the basis of EXAFS measurements showing that the coordination number of ∼3.4 for Ru−N bonds[40] and a simulation study[47] showing that Ru-N_4 is expected to show superior performance as compared with Ru-N_3. As the first reaction step we considered the interaction between H_2 and the active site. The adsorbed H_2 molecule was found to be unstable on the Ru-N_4 site, decomposing spontaneously into two H atoms as shown in Figure S2. This indicates that the Heyrovsky step ($2H^* \rightarrow H_2$) is difficult and the catalyst's NRR selectivity is promising. To understand HER on the catalyst studied, we examined the electrochemical Volmer reaction ($H_3O^+ + e^- \rightarrow *H + H_2O$). This reaction is a fundamental step in HER and generally used to determine HER activity.[48,49] Because the Ru-N_4 exhibits high NRR performance under acidic conditions,[40] we studied the acidic Volmer step from a H_3O^+ ion solvated in a water layer near the catalyst surface. Figure 1a and Table S3 show that, according to the constant potential GCE-DFT calculations, the Volmer reaction has a high activation energy of 1.32 eV at 0 V_{SHE} but is thermodynamically feasible as seen from the exergonic reaction free energies (ΔE_r). The reaction becomes both thermodynamically and kinetically more accessible as the electrode potential decreases. The comparison of canonical fixed-charge or constant-potential GCE-DFT calculations clearly shows that the activation and reaction energies are potential-dependent and that the two methods yield similar results only at $U = -0.2$ V_{SHE} for the Volmer reaction. Interestingly, the activation barriers are more sensitive than reaction thermodynamics to changes in the electrode potential. This behavior is analyzed in

https://doi.org/10.1021/acscatal.1c05820
ACS Catal. 2022, 12, 2505−2512

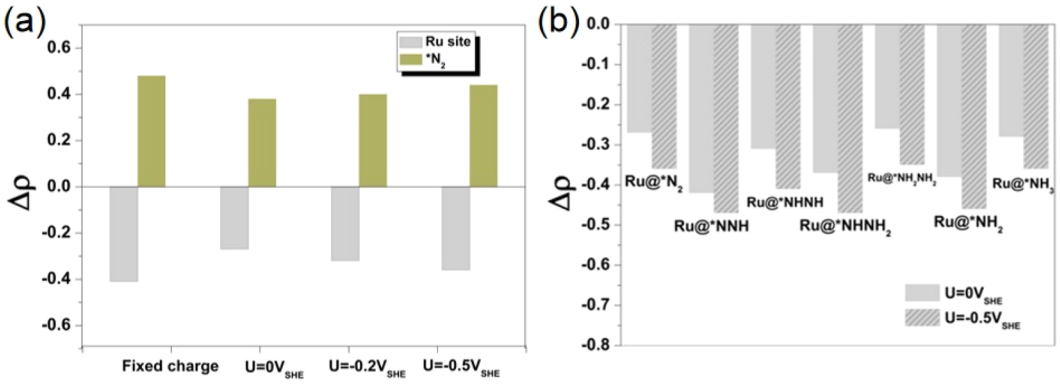

Figure 2. (a) The charge variation ($\Delta\rho$ = ρN_2(adsorption) − ρN_2(gas)) of the adsorbed *N_2 on Ru-N_4 site and the corresponding $\Delta\rho$ ($\Delta\rho$ = ρRu(Ru@N_2) − ρRu(bare)) of the Ru site occupied by *N_2 intermediate species (Ru@N_2) with fixed-charge and constant-potential(U). (b) The $\Delta\rho$ ($\Delta\rho$ = ρRu(Ru@N_xH_y) − ρRu(bare)) of the Ru site occupied by NRR intermediate species (Ru@N_xH_y) at different electrode potentials. Positive values correspond to accumulation of charge.

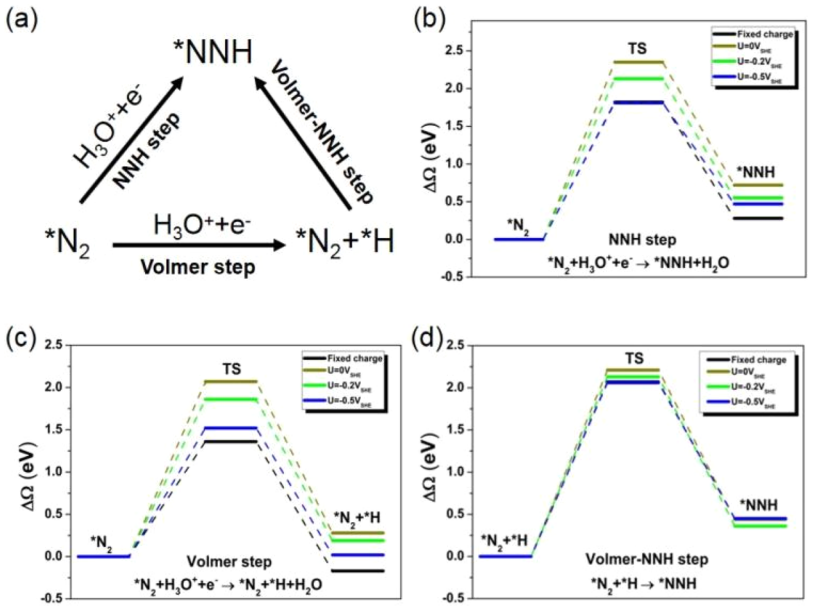

Figure 3. (a) The possible pathways for the first PCET in NRR. (b–d) Corresponding energy diagrams.

detail in the Supporting Information Section S6 and can be attributed to the electrode's low density of states and the water reorganization during the reaction.

The first NRR step, N_2 adsorption on the active site, is nominally a chemical reaction and expected to be independent of the electrode potential. Figure 1b along with Tables S2–S3, however, show that N_2 adsorbs strongly at the Ru-N_4 site, and the adsorption energy depends on the electrode potential. The constant potential treatment predicts stronger adsorption than the constant charge calculation by approximately 0.5 eV. The large difference in adsorption energies between the two methods is due to the $\Phi_e \Delta N_e$ term in the definition of grand free energies as discussed in the Supporting Information Section S1 (Φ_e is the absolute electrode potential and ΔN_e the change in the number of electrons in the system). The potential-dependency of N_2 adsorption can be understood by analyzing the Bader charges given in Figure 2. The Bader charge analysis reveals that an electron transfer from Ru to *N_2 forming a π backbond[17,18,50] occurs during adsorption. This leads to stronger N_2 adsorption and activation. Figure 2a shows that the Ru-N_4 site can promote N_2 activation through electron donation at reducing potentials and, in particular, the charge transfer between Ru and N_2 depends on the electrode potential. The explicit potential dependency of the adsorption energy and charge transfer also demonstrates that using GCE-DFT is warranted even for nominally chemical steps.

The results in Figure 1 and Tables S2–S3 show that the adsorption energy of N_2 is more exothermic than the Volmer reaction energy at all considered potentials. HER is also kinetically limited as the Volmer reaction has a sizable barrier compared to, e.g., platinum[51] where the Volmer reaction has low barriers and the HER is limited by the Heyrovsky step. On Ru-N_4, the N_2 adsorption is favored over H adsorption, at least when transport limitations are omitted, and given the high Volmer barrier it is unlikely that the Ru-N_4 is active toward HER under the considered reaction conditions. Instead, NRR and HER may proceed simultaneously having coadsorbed *H and *N_xH_y intermediates present and interacting with each other.[52] Therefore, we addressed HER along the NRR pathway, with different possible coadsorption configurations shown in Figures 3 and 4.

https://doi.org/10.1021/acscatal.1c05820
ACS Catal. 2022, 12, 2505−2512

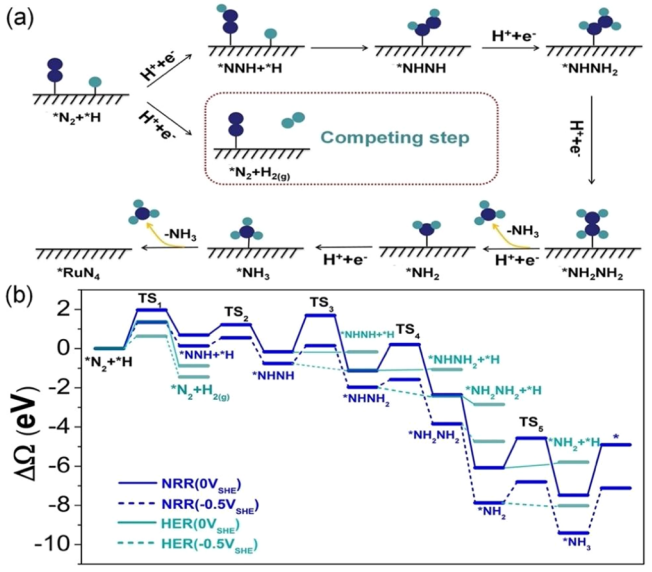

Figure 4. (a) Competing NRR (blue) and HER (green) pathways and (b) the associated grand free energies.

Initially, we considered three distinct elementary steps from an adsorbed $*N_2$ configuration toward a NNH intermediate, shown in Figure 3a. These steps are the NNH step, the Volmer step, and the Volmer-NNH step. Both NNH and Volmer steps are electrochemical PCET reactions depending strongly on the electrode potential (see Figure 3), whereas the Volmer-NNH step is a chemical reaction step. Figure 3b shows that the NNH step is highly unfavored with $E_a > 1.75$ eV and $\Delta E_r = 0.5$ eV even at -0.5 V_{SHE}. The high barrier and endothermicity are in line with the general understanding that the first PCET step producing *NNH hinders NRR kinetically.[8]

The Volmer step leading to coadsorbed $*N_2$ and *H is thermoneutral at -0.5 V_{SHE} (see Figure 3c) due to the presence of $*N_2$ and the decreased charge on the Ru center. According to the commonly applied Volcano analysis,[53−55] nearly thermoneutral hydrogen adsorption indicates that $*N_2$-Ru-N_4 is close to an ideal HER catalyst. Interestingly, the presence of $*N_2$ significantly increases the reaction barrier for the Volmer step compared with the barrier on the empty Ru-N_4 site as can be seen by comparing the grand free energy profiles in Figures 1a and 3c. For instance, at -0.2 V_{RHE}, $*N_2$ increases the Volmer barrier from 0.85 to 1.85 eV and makes the reaction thermodynamically unfavorable by changing the reaction energy from -1.0 to 0.4 eV. This comparison clearly demonstrates that NRR/HER competition cannot be explained by reaction thermodynamics alone or a simple description for the active site. The Volmer reaction barriers also exemplify the importance of GCE-DFT as the constant charge barriers with and without $*N_2$ differ by 0.25 eV, whereas constant potential barriers show a ∼0.75 eV energy span.

Comparison of the grand free energy profiles in Figure 3b,c shows that the coadsorption of $*N_2$+*H is both kinetically and thermodynamically more favorable than direct formation of *NNH. The alternative mechanism leading to *NNH through coadsorbed *H and $*N_2$, the Volmer-NNH step, is highly unfavorable, and the activation barrier is higher than 2 eV. The first PCET step is therefore the Volmer step despite a sizable barrier. The coadsorbed ($*N_2$+*H) structure is expected to exist on the Ru-N_4 site without proceeding to *NNH through the Volmer-NNH step. Similar coadsorption structures have been previously identified for other SAC-catalyzed reactions, and they are known to greatly impact activity and selectivity of the CO_2 reduction reaction.[56,57]

We examined alternative PCET pathways to form *NNH and other NRR intermediates as shown in Figure 4a. The

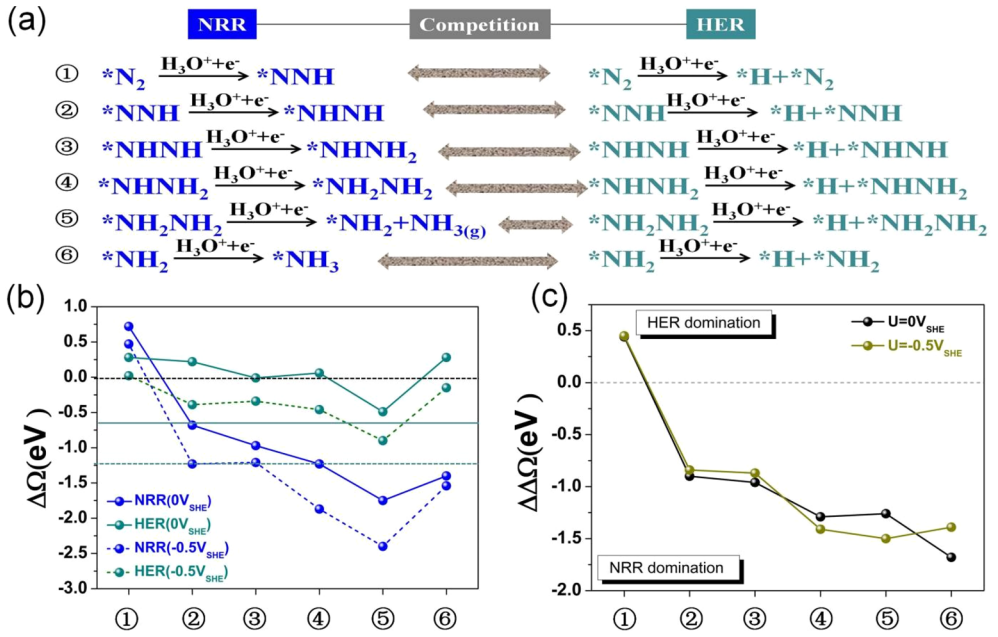

Figure 5. (a) The competing PCET steps in NRR and HER, and (b) the corresponding reaction energies. The black dashed line depicts optimal HER ($\Delta\Omega = 0$). The dark cyan solid and dashed lines are $\Delta\Omega$ value of Volmer reaction on pure Ru-N_4 site at 0 V_{SHE} and -0.5 V_{SHE}, respectively. (c) The thermodynamic selectivity between NRR and HER. The selectivity refers to the reaction energy difference ($\Delta\Delta\Omega$) between NRR and Volmer steps. The numbering in (b) and (c) corresponds to the steps in (a). The atom configurations are displayed in Figure S4.

https://doi.org/10.1021/acscatal.1c05820
ACS Catal. 2022, 12, 2505−2512

second PCET step leads to *NNH via the N_2 hydrogenation step ($*N_2+*H+H_3O^+ + e^- \rightarrow *NNH+*H+H_2O$) or H_2 via the Heyrovsky step ($*N_2+*H+H_3O^+ + e^- \rightarrow *N_2+H_{2(g)}+H_2O$). In the presence of *H, the reduction of $*N_2$ to *NNH is slightly thermodynamically and kinetically favored over the reduction without adsorbed *H as can be seen by comparing the energy profiles in Figures 3b and 4b. The Heyrovsky step, however, is both kinetically and thermodynamically more feasible than the N_2 hydrogenation step, as shown in Figure 4b, and thus, H_2 is readily formed (see Figure S3 for atomic structures).

At 0 V_{SHE}, the Heyrovsky step is already highly exergonic but there is a large activation energy of 1.4 eV. Decreasing the potential to −0.5 V_{SHE} makes the step even more exergonic and lowers the activation energy below 0.75 eV. These results demonstrate that the adsorbed $*N_2$ facilitates the Heyrovsky step compared with the empty Ru-N_4 site where it is unfeasible because of spontaneous H_2 dissociation. The effect of $*N_2$ can again be understood by considering the Bader charges given in Figure 2b. The charge analysis shows that the Ru atom becomes more positively charged upon $*N_2$ adsorption, which in turn hinders H_2 dissociation. More specifically, the π back-donation from Ru to N_2 leads to vacant d-states thereby decreasing the electron transfer to the σ^* orbital of H_2 and consequently stabilizing the formation of the H−H bond.[20,58,59]

The results in Figures 2−3 and Tables S2−S3 show that HER proceeds more easily than NRR both in the presence and absence of $*N_2$ on the Ru-N_4 site. The Volmer reaction has a much higher barrier than the Heyrovsky step indicating that NRR/HER selectivity depends on whether *H or $*N_xH_y$ is formed. We therefore compared further PCET steps leading to either *H or various nitrogen-containing intermediates on the Ru-N_4 site along the pathways displayed in Figure 4a.

The result in Figure 4b and Table S2 show that forming *NNH is more demanding than *H and H_2. However, once *NNH is formed, then NRR is at least thermodynamically more favorable than HER as shown in Figure 4b. Figures 4b and 5 show that the formation of any NRR reaction intermediate after *NNH is highly exergonic and has a lower barrier than the corresponding Volmer step. While we have not computed Volmer barriers in the presence of all $*N_xH_y$ intermediates, Figure S9 shows a strong correlation between the Volmer reaction energies and barriers. This allows us to estimate the Volmer reaction barrier which is ∼1.75 eV when the step thermoneutral. At 0 V_{SHE}, the Volmer barriers are higher than or equal to the NRR barriers (apart from *NNH formation), whereas at −0.5 V_{SHE}, NRR has lower barriers for all steps after *NNH. Combining the thermodynamic and kinetic data in Figures 4b, 5, and S9 shows that all PCET steps after *NNH favor the formation of NRR intermediates such as *NHNH, $*NHNH_2$, $*NH_2NH_2$, $*NH_2$, and $*NH_3$ rather than *H. This demonstrates that the Volmer step limits HER activity of the Ru-N_4 hosting any $*N_xH_y$ intermediate. The weakened hydrogen adsorption in the presence of $*N_xH_y$ species is caused by the accumulation of positive charge on the Ru atom as shown in Figures 2b and S3.

The NRR/HER selectivity for the PCET steps in Figure 5a is further analyzed by comparing the reaction free energies ($\Delta\Omega$) between NRR and Volmer steps in the presence of different N_xH_y intermediates. We hypothesize that there exists a window of reaction energies where HER is thermodynamically preferred. If the reaction energy difference, $\Delta\Delta\Omega$, between NRR and Volmer steps is >0, HER is preferred as the Volmer reaction is thermodynamically more favorable than the hydrogenation of a nitrogen species. Conversely, when $\Delta\Delta\Omega < 0$, NRR is preferred. Figure 5c shows that $\Delta\Delta\Omega > 0$ only for the first PCET step at potentials relevant for NRR. This indicates that the first PCET step before *NNH formation determines thermodynamic selectivity toward NRR or HER. This conclusion is also supported by the computed and estimated activation energies Tables S2−S3 and Figure S9, which show the HER is the kinetically preferred step only before *NNH formation.

The first PCET forming *NNH is clearly the rate-limiting step, and the Volmer step is more facile. Our results, however, indicate that the Volmer barrier increases when the catalyst is less negatively charged because of $*N_2$ withdrawing electrons from the active site. A recent DFT study suggests that "non-innocent" spectators adsorbed on single-atom catalysts can profoundly affect their catalytic performance.[60] To see if these spectators modify NRR efficiency, we tested the influence of $*N_2$ on the "unreactive side" of Ru-N_4. The results given in Figure S6 show that adding another $*N_2$ is thermodynamically favorable. The additional $*N_2$ increases the activation barriers for both Volmer and *NNH formation steps making them less thermodynamically favored as shown in Figure S8 and Table S2. We note that the constant charge and constant potential barriers and reaction energies for a given step can differ by up to ∼1 eV, making the use of GCE-DFT a necessity. Most importantly, the reaction barrier difference ($\Delta\Delta\Omega^{\ddagger} = \Delta\Omega^{\ddagger}_{NNH} - \Delta\Omega^{\ddagger}_{Volmer}$) at −0.2 V_{RHE} decreases from 0.27 to 0.16 eV when a "non-innocent" $*N_2$ ligand is present. These results indicate that the second $*N_2$ will decrease the overall activity but increase selectivity toward NRR since *NNH formation kinetics becomes more competitive with HER.

We found that HER/NRR competition on the Ru-N_4 catalyst is complex and sensitive to the presence of NRR intermediates at the active site. N_2 adsorbs strongly and more favorably than H at the active Ru-N_4 site. The unusually strong N_2 adsorption on Ru-N_4 distinguishes this catalyst from the widely studied Fe-N_4 catalyst where weak N_2 and stronger H adsorption under reducing conditions lead to poor NRR selectivity.[60] All our computed thermodynamic and kinetic data for Ru-N_4 support that, among different NRR steps, the first PCET step leading to *NNH is clearly the rate and selectivity limiting step. The reacting $*N_2$ also has a profound effect on the HER kinetics as its presence increases the Volmer barrier from ∼0.75 eV to ∼1.9 eV at −0.2 V_{RHE}. In fact, the presence of any $*N_xH_y$ species at the active site suppresses *H formation by making the Volmer step kinetically and thermodynamically more difficult than without coadsorbates. The Heyrovsky step, on the other hand, is facilitated by the presence of NRR intermediates and additional $*N_2$ underneath the active site makes NRR kinetics competitive with HER. Thus, it is crucial to consider the impact of $*N_xH_y$ intermediates on HER energetics when assessing the competition between HER and NRR. The charge analysis in Figure 2 also shows that the charge transfer from Ru plays an important, potential-dependent role on thermodynamics and kinetics warranting the use of GCE-DFT.

If we assume that the experimentally observed[40] 30% selectivity at −0.2 V_{RHE} on Ru-N_4 can be attributed to competition between *NNH and *H formation rates (k_{NNH} and k_{Volmer}), the Faradaic efficiency (FE) can be approximated as

https://doi.org/10.1021/acscatal.1c05820
ACS Catal. 2022, 12, 2505−2512

$$\mathrm{FE} = \frac{j_{\mathrm{NRR}}}{j_{\mathrm{HER}} + j_{\mathrm{NRR}}} \approx \frac{k_{\mathrm{NNH}} n_{e,\mathrm{NRR}}}{k_{\mathrm{NNH}} n_{e,\mathrm{NRR}} + k_{\mathrm{Volmer}} n_{e,\mathrm{NRR}}} \quad (1)$$

where $n_{e,\mathrm{NRR}} = 6$ and $n_{e,\mathrm{HER}} = 2$ are the number of electrons transferred in the total NRR and HER processes, respectively. The *NNH and *H formation rates can be computed using the GCE transition station theory[61] as

$$k_i(U) = \frac{k_B T}{h} \exp\left[-\frac{\Delta\Omega^{\ddagger}(U)}{k_B T}\right] \quad (2)$$

where $\Delta\Omega^{\ddagger}(U)$ is the potential-dependent grand free energy barrier. After inserting eq 2 into eq 1, we can evaluate which barrier difference, $\Delta\Delta\Omega^{\ddagger} = \Delta\Omega^{\ddagger}_{\mathrm{NNH}} - \Delta\Omega^{\ddagger}_{\mathrm{Volmer}}$, leads to a given FE. Evaluation of $\Delta\Delta\Omega^{\ddagger}$ for FE = 30% measured at T = 298 K, gives $\Delta\Delta\Omega^{\ddagger}$ (U = 0.2 V_{SHE}) ≈ 0.06 eV. By comparing this effective barrier to our computed reaction barriers for *NNH formation and the Volmer steps allows inferring the importance of $*N_2$+*H coadsorption and the $*N_2$ ligand. Including both coadsorbed $*N_2$+*H and another $*N_2$ ligand gives $\Delta\Delta\Omega^{\ddagger}$ = 0.16 eV while neglecting these effects gives $\Delta\Delta\Omega^{\ddagger}$ = 0.75 eV. This comparison shows that accounting for both coadsorption and the additional $*N_2$ ligand is required to properly explain the experimental NRR selectivity. We note that $\Delta\Delta\Omega^{\ddagger}$ = 0.16 eV is already close to the typical GGA-DFT error of ∼0.15 eV for ammonia synthesis.[62] The difference between the computed $\Delta\Delta\Omega^{\ddagger}$ value and the experimental effective barrier ($\Delta\Delta\Omega^{\ddagger} \approx$ 0.06 eV) can also result from a simplified solvent model used in calculations or omission of electrolyte ions, which are known to affect NRR selectivity and activity in experiments as discussed in the introduction. While high computed NRR barriers are partially in line with experimentally measured low NRR current densities, extracting absolute barriers current densities from DFT calculations usually contains large inaccuracies,[51] whereas relative quantities are more reliable. Despite the limitations in the computational model, our results unequivocally show that coadsorbed $*N_xH_y$ and $*N_2$-ligand suppress HER and that even modest selectivity toward NRR cannot be achieved without the presence of N_2-derived species at the Ru-N_4 active site.

Our results can also guide the search for a more selective and active NRR catalyst: higher NRR activity and selectivity requires suppressing hydrogen adsorption (Volmer step) at the active site occupied by $*N_2$ while simultaneously enhancing $*N_2$ protonation. On the catalyst studied, this cannot be achieved by only restricting the transport of protons because steps leading to either $*N_2$+*H or H_2 are easier than N_2 hydrogenation. Instead, NRR enhancement requires controlling the PCET kinetics and thermodynamics of the step leading to either *H or *NNH. Such selective control over the PCET NRR chemistry could be achieved by depositing hydrogen bonding moieties or proton donors that are *spatially distant* from the Ru-N_4 center to either selectively stabilize *NNH or favor hydrogenation of $*N_2$, respectively. Similar strategies to selectively facilitate NRR are employed by a natural nitrogenase entzyme,[32] in the promising molecular crowding approach,[16] methanol-mediated NRR,[63] and suggested for Li^+-mediated NRR in a "solid electrolyte interface" -like layer near the electrode.[64] For other electrocatalytic reactions, such as O_2[65] and CO_2[66] reduction, molecular modifiers bound to the surface have been found to efficiently control the interfacial microenvironment and the PCET chemistry.[67,68] It should also be noticed that the identified importance of noninnocent ligands or coadsorbates is not limited to NRR and RuN_4 but may also be crucial for other SACs[43,52] and in CO_2RR.[56,57]

In summary, we studied computationally the competition between NRR and HER on the promising Ru-N_4 SAC using constant potential DFT simulations and a hybrid solvent model. Our results show that the catalyst studied exhibits stronger affinity toward N_2 than H adsorption, suggesting that NRR could be preferred. The N_2 adsorption hinders hydrogen deposition through the Volmer step compared to the empty Ru-N_4 site. However, the first Volmer step after N_2 adsorption is still more favorable than N_2 hydrogenation. Once $*N_2$ and *H are coadsorbed, H_2 is easily generated through the Heyrovsky step whereas the formation of the first NRR intermediate, *NNH, is kinetically and thermodynamically more difficult limiting the overall NRR activity and selectivity. If one can overcome the bottleneck of *NNH formation, HER is significantly suppressed until NH_3 is released. The presence of $*N_2$ and NRR species significantly suppresses HER activity, and we suggest that the experimentally observed 30% selectivity toward NRR on Ru-N_4 results from the hindered Volmer step in the presence of adsorbed NRR intermediates and a "non-innocent" $*N_2$ ligand. Overall, our results reveal the complex competition between NRR and HER, the role of coadsorption on SACs, the $*N_2$ ligand, and the importance of potential-dependent thermodynamics, kinetics, and charge transfer captured with GCE-DFT. On the basis of this detailed insight, we propose that the NRR selectivity can be increased by restricting N_2 and H coadsorption on SACs through spatially distant proton-donating or hydrogen-bonding moieties to favor *NNH formation.

■ ASSOCIATED CONTENT

Supporting Information

The Supporting Information is available free of charge at https://pubs.acs.org/doi/10.1021/acscatal.1c05820.

S1: Calculation details. S2: Structure diagrams. S3: Vibrational Frequencies. S4: Additional results for the systems with two adsorbed N_2. S5: Tabulated reaction energies and barrier heights. S6: System charge as a function of the electrode potential for different structures (PDF)

■ AUTHOR INFORMATION

Corresponding Author

Karoliina Honkala − *Department of Chemistry, Nanoscience Center, University of Jyväskylä, FI-40014 Jyväskylä, Finland;* orcid.org/0000-0002-3166-1077; Email: karoliina.honkala@jyu.fi

Authors

Tongwei Wu − *Department of Chemistry, Nanoscience Center, University of Jyväskylä, FI-40014 Jyväskylä, Finland; State Key Laboratory of Electronic Thin Films and Integrated Devices and Institute of Fundamental and Frontier Sciences, University of Electronic Science and Technology of China, Chengdu, Sichuan 610054, China*

Marko M. Melander − *Department of Chemistry, Nanoscience Center, University of Jyväskylä, FI-40014 Jyväskylä, Finland;* orcid.org/0000-0001-7111-1603

Complete contact information is available at:

https://doi.org/10.1021/acscatal.1c05820
ACS Catal. 2022, 12, 2505−2512

https://pubs.acs.org/10.1021/acscatal.1c05820

Notes

Optimized adsorption and transition state structures are freely available on https://gitlab.jyu.fi/mamimela/nrr_data.
The authors declare no competing financial interest.

■ ACKNOWLEDGMENTS

T.W. acknowledges the support by the National Natural Science Foundation of China (No. 11874005), the China National Postdoctoral Program for Innovative Talents (No. BX2021053), China Postdoctoral Science Foundation (No.2021M700680) and China Scholarship Council (No. 201906070128). T.W. also acknowledges the support of the Shang Hai Tong Ji Gao Ting Yao Environment Science and Technology Development Foundation. M.M.M. and K.H. gratefully acknowledge support by the Academy of Finland (grant numbers 317739 and 338228), and the Jane and Aatos Erkko Foundation (funding to the LACOR project). We thank Dr. Laura Laverdure for careful reading of the manuscript. The computational resources were provided by the CSC−IT Center for Science, Espoo, Finland (https://www.csc.fi/en/) and the FGCI - Finnish Grid and Cloud Infrastructure.

■ REFERENCES

(1) Schlögl, R. Catalytic Synthesis of Ammonia—A "Never-Ending Story. *Angew. Chem., Int. Ed.* **2003**, *42*, 2004−2008.
(2) Smil, V. Detonator of the Population Explosion. *Nature* **1999**, *400*, 415.
(3) Hellman, A.; Honkala, K.; Dahl, S.; Christensen, C. H.; Nørskov, J. K. Ammonia Synthesis: State of the Bellwether Reaction in Comprehensive Inorganic Chemistry II (Second Edition): From Elements to Applications. *Elsevier* **2013**, 459−474.
(4) Smith, C.; Hill, A. K.; Torrente-Murciano, L. Current and Future Role of Haber-Bosch Ammonia in a Carbon-free Energy Landscape. *Energy Environ. Sci.* **2020**, *13*, 331−344.
(5) Chen, J. G.; Crooks, R. M.; Seefeldt, L. C.; Seefeldt, L. C.; Bren, K. L.; Bullock, R. M.; Darensbourg, R. Y.; Holland, P. L.; Hoffman, B.; Janik, M. J.; Schrock, R. R.; et al. Beyond Fossil Fuel-driven Nitrogen Transformations. *Science* **2018**, *360*, eaar6611.
(6) Qing, G.; Ghazfar, R.; Jackowski, S. T.; Habibzadeh, F.; Ashtiani, M. M.; Chen, C.-P.; Smith, M. R., III; Hamann, T. W. Recent Advances and Challenges of Electrocatalytic N_2 Reduction to Ammonia. *Chem. Rev.* **2020**, *120*, 5437−5516.
(7) Wu, T.; Zhu, X.; Xing, Z.; Mou, S.; Li, C.; Qiao, Y.; Liu, Q.; Luo, Y.; Shi, X.; Zhang, Y.; Sun, X. Greatly Improving Electrochemical N_2 Reduction over TiO_2 Nanoparticles by Iron Doping. *Angew. Chem., Int. Ed.* **2019**, *58*, 18449−18453.
(8) Ren, Y.; Yu, C.; Tan, X.; Huang, H.; Wei, Q.; Qiu, J. Strategies to Suppress Hydrogen Evolution for Highly Selective Electrocatalytic Nitrogen Reduction: Challenges and Perspectives. *Energy Environ. Sci.* **2021**, *14*, 1176−1193.
(9) Kibsgaard, J.; Nørskov, J. K.; Chorkendorff, I. The Difficulty of Proving Electrochemical Ammonia Synthesis. *ACS Energy Lett.* **2019**, *4*, 2986−2988.
(10) Song, Y.; Johnson, D.; Peng, R.; Hensley, D. K.; Bonnesen, P. V.; Liang, L.; Huang, J.; Yang, F.; Zhang, F.; Qiao, R.; Baddorf, A. P.; Tschaplinski, T. J.; Engle, N. L.; Hatzell, M. C.; Wu, Z.; Cullen, D. A.; Meyer, H. M.; Sumpter, B. G.; Rondinone, A. J. A Physical Catalyst for the Electrolysis of Nitrogen to Ammonia. *Sci. Adv.* **2018**, *4*, e1700336.
(11) Wu, T.; Zhao, H.; Zhu, X.; Xing, Z.; Liu, Q.; Liu, T.; Gao, S.; Lu, S.; Chen, G.; Asiri, A. M.; Zhang, Y.; Sun, X. Identifying the Origin of Ti^{3+} Activity toward Enhanced Electrocatalytic N_2 Reduction over TiO_2 Nanoparticles Modulated by Mixed-Valent Copper. *Adv. Mater.* **2020**, *32*, 2000299.
(12) Zhang, L.; Ding, L.-X.; Chen, G.-F.; Yang, X.; Wang, H. Ammonia Synthesis Under Ambient Conditions: Selective Electroreduction of Dinitrogen to Ammonia on Black Phosphorus Nanosheets. *Angew. Chem., Int. Ed.* **2019**, *58*, 2612−2616.
(13) Yu, X.; Han, P.; Wei, Z.; Huang, L.; Gu, Z.; Peng, S.; Ma, J.; Zheng, G. Boron-Doped Graphene for Electrocatalytic N_2 Reduction. *Joule* **2018**, *2*, 1610−1622.
(14) Tang, C.; Qiao, S. Z. How to Explore Ambient Electrocatalytic Nitrogen Reduction Reliably and Insightfully. *Chem. Soc. Rev.* **2019**, *48*, 3166−3180.
(15) Xue, Z.-H.; Zhang, S.-N.; Lin, Y.-X.; Su, H.; Zhai, G.-Y.; Han, J.-T.; Yu, Q.-Y.; Li, X.-H.; Antonietti, M.; Chen, J.-S. Electrochemical Reduction of N_2 into NH_3 by Donor−acceptor Couples of Ni and Au Nanoparticles with a 67.8% Faradaic Efficiency. *J. Am. Chem. Soc.* **2019**, *141*, 14976−14980.
(16) Guo, Y.; Gu, J.; Zhang, R.; Zhang, S.; Li, Z.; Zhao, Y.; Huang, Z.; Fan, J.; Chen, Z.; Zhi, C. Molecular Crowding Effect in Aqueous Electrolytes to Suppress Hydrogen Reduction Reaction and Enhance Electrochemical Nitrogen Reduction. *Adv. Energy Mater.* **2021**, *11*, 2101699.
(17) Liu, X.; Jiao, Y.; Zheng, Y.; Jaroniec, M.; Qiao, S.-Z. Building Up a Picture of the Electrocatalytic Nitrogen Reduction Activity of Transition Metal Single-Atom Catalysts. *J. Am. Chem. Soc.* **2019**, *141*, 9664−9672.
(18) Liu, C.; Li, Q.; Wu, C.; Zhang, J.; Jin, Y.; MacFarlane, D. R.; Sun, C. Single-Boron Catalysts for Nitrogen Reduction Reaction. *J. Am. Chem. Soc.* **2019**, *141*, 2884−2888.
(19) Lv, X.; Wei, W.; Huang, B.; Dai, Y.; Frauenheim, T. High-throughput Screening of Synergistic Transition Metal Dual-atom Catalysts for Efficient Nitrogen Fixation. *Nano Lett.* **2021**, *21*, 1871−1878.
(20) Choi, C.; Back, S.; Kim, N.-Y.; Lim, Y.; Kim, Y.-H.; Jung, Y. Suppression of Hydrogen Evolution Reaction in Electrochemical N_2 Reduction using Single-atom Catalysts: a Computational Guideline. *ACS Catal.* **2018**, *8*, 7517−7525.
(21) Montoya, J. H.; Tsai, C.; Vojvodic, A.; Nørskov, J. K. The Challenge of Electrochemical Ammonia Synthesis: A New Perspective on the Role of Nitrogen Scaling Relations. *ChemSusChem* **2015**, *8*, 2180−2186.
(22) Singh, A. R.; Rohr, B. A.; Statt, M. J.; Schwalbe, J. A.; Cargnello, M.; Nørskov, J. K. Strategies toward Selective Electrochemical Ammonia Synthesis. *ACS Catal.* **2019**, *9*, 8316−8324.
(23) Hao, Y.-C.; Guo, Y.; Chen, L.-W.; Shu, M.; Wang, X.-U.; Bu, T.-A.; Gao, W.-Y.; Zhang, N.; Su, X.; Feng, X.; Zhou, J.-W.; Wang, B.; Hu, C.-W.; Yin, A.-X.; Si, R.; Zhang, Y.-W.; Yan, C.-H. Promoting nitrogen electroreduction to ammonia with bismuth nanocrystals and potassium cations in water. *Nat. Catal.* **2019**, *2*, 448−456.
(24) Drazevic, E.; Skúlason, E. Are There Any Overlooked Catalysts for Electrochemical NH_3 Synthesis − New Insights from Analysis of Thermochemical Data. *iScience* **2020**, *23*, 101803.
(25) Van der Ham, C. J.; Koper, M. T.; Hetterscheid, D. G. Challenges in Reduction of Dinitrogen by Proton and Electron Transfer. *Chem. Soc. Rev.* **2014**, *43*, 5183−5191.
(26) Bagger, A.; Wan, H.; Stephens, I. E.; Rossmeisl, J. Role of Catalyst in Controlling N_2 Reduction Selectivity: A Unified View of Nitrogenase and Solid Electrodes. *ACS Catal.* **2021**, *11*, 6596−6601.
(27) Hou, J.; Yang, M.; Zhang, J. Recent Advances in Catalysts, Electrolytes and Electrode Engineering for the Nitrogen Reduction Reaction under Ambient Conditions. *Nanoscale* **2020**, *12*, 6900−6920.
(28) Suryanto, B. H.; Matuszek, K.; Choi, J.; Hodgetts, R. Y.; Du, H.-L.; Bakker, J. M.; Kang, C. S.; Cherepanov, P. V.; Simonov, A. N.; MacFarlane, D. R. Nitrogen Reduction to Ammonia at High Efficiency and Rates Based on a Phosphonium Proton Shuttle. *Science* **2021**, *372*, 1187−1191.
(29) Hu, L.; Xing, Z.; Feng, X. Understanding the Electrocatalytic Interface for Ambient Ammonia Synthesis. *ACS Energy Lett.* **2020**, *5*, 430−436.

(30) Nilsson, A.; Stephens, I. Section 5. Sustainable N_2 reduction. *Research needs towards sustainable production of fuels and chemicals*; Nørksov, J. K., https://www.energy-x.eu/research-needs-report/ (accessed November 11, 2021).
(31) Qiu, W.; Xie, X.-Y.; Qiu, J.; Fang, W.-H.; Liang, R.; Ren, X.; Ji, X.; Cui, G.; Asiri, A. M.; Cui, G.; Tang, B.; Sun, X. High-performance Artificial Nitrogen Fixation at Ambient Conditions using a Metal-free Electrocatalyst. *Nat. Commun.* **2018**, *9*, 3485.
(32) Kang, W.; Lee, C. C.; Jasniewski, A. J.; Ribbe, M. W.; Hu, Y. Structural Evidence for a Dynamic Metallocofactor during N_2 Reduction by Mo-nitrogenase. *Science* **2020**, *368*, 1381−1385.
(33) Zhang, R.; Wang, Q. H.; Luo, Z. Y.; Fang, M. X.; Cen, K. F. Competition and Inhibition Effects during Coal Char Gasification in the Mixture of H_2O and CO_2. *Energy fuel.* **2013**, *27*, 5107−5115.
(34) Chevillard, C.; Cárdenas, M. L.; Cornish-Bowden, A. The Competition Plot: a Simple Test of Whether two Reactions Occur at the Same Active Site. *Biochem. J.* **1993**, *289*, 599−604.
(35) Chen, Z. W.; Yan, J. M.; Jiang, Q. Single or Double: which is the Altar of Atomic Catalysts for Nitrogen Reduction Reaction? *Small Methods* **2019**, *3*, 1800291.
(36) Guo, X.; Gu, J.; Lin, S.; Zhang, S.; Chen, Z.; Huang, S. Tackling the Activity and Selectivity Challenges of Electrocatalysts toward the Nitrogen Reduction Reaction via Atomically Dispersed Biatom Catalysts. *J. Am. Chem. Soc.* **2020**, *142*, 5709−5721.
(37) Qiu, Y.; Peng, X.; Lü, F.; Mi, Y.; Zhuo, L.; Ren, J.; Liu, X.; Luo, J. Single-Atom Catalysts for the Electrocatalytic Reduction of Nitrogen to Ammonia under Ambient Conditions. *Chem−Asian J.* **2019**, *14*, 2770−2779.
(38) Jiao, D.; Liu, Y.; Cai, Q.; Zhao, J. Coordination Tunes the Activity and Selectivity of the Nitrogen Reduction Reaction on Single-atom Iron catalysts: A Computational Study. *J. Mater. Chem. A* **2021**, *9*, 1240−1251.
(39) Zhao, J.; Chen, Z. Single Mo Atom Supported on Defective Boron Nitride Monolayer as an Efficient Electrocatalyst for Nitrogen Fixation: A Computational Study. *J. Am. Chem. Soc.* **2017**, *139*, 12480−12487.
(40) Geng, Z.; Liu, Y.; Kong, X.; Li, P.; Li, K.; Liu, Z.; Du, J.; Shu, M.; Si, R.; Zeng, J. Achieving a Record-high Yield Rate of 120.9 for N_2 Electrochemical Reduction over Ru Single-atom Catalysts. *Adv. Mater.* **2018**, *30*, 1803498.
(41) Zhao, W.; Zhang, L.; Luo, Q.; Hu, Z.; Zhang, W.; Smith, S.; Yang, J. Single Mo_1 (Cr_1) Atom on Nitrogen-doped Graphene Enables Highly Selective Electroreduction of Nitrogen into Ammonia. *ACS Catal.* **2019**, *9*, 3419−3425.
(42) Lü, F.; Zhao, S.; Guo, R.; He, J.; Peng, X.; Bao, H.; Fu, J.; Han, L.; Qi, G.; Luo, J.; Tang, X.; Liu, X. Nitrogen-coordinated Single Fe Sites for Efficient Electrocatalytic N_2 Fixation in Neutral Media. *Nano Energy* **2019**, *61*, 420−427.
(43) Han, L.; Liu, X.; Chen, J.; Lin, R.; Liu, H.; Lu, F.; Bak, S.; Liang, Z.; Zhao, S.; Stavitski, E.; Luo, J.; Adzic, R. R.; Xin, H. L. Atomically Dispersed Molybdenum Catalysts for Efficient Ambient Nitrogen Fixation. *Angew. Chem., Int. Ed.* **2019**, *131*, 2343−2347.
(44) Melander, M. M. Grand Canonical Ensemble Approach to Electrochemical Thermodynamics, Kinetics, and Model Hamiltonians. *Current Opinion in Electrochemistry* **2021**, *29*, 100749.
(45) Schwarz, K.; Sundararaman, R. The Electrochemical Interface in First-principles Calculations. *Surf. Sci. Rep.* **2020**, *75*, 100492.
(46) Melander, M. M.; Kuisma, M. J.; Christensen, T. E. K.; Honkala, K. Grand-canonical Approach to Density Functional Theory of Electrocatalytic Systems: Thermodynamics of Solid-liquid Interfaces at Constant Ion and Electrode Potentials. *J. Chem. Phys.* **2019**, *150*, 041706.
(47) Ji, Y.; Li, Y.; Dong, H.; Ding, L.; Li, Y. Ruthenium Single-Atom Catalysis for Electrocatalytic Nitrogen Reduction Unveiled by Grand Canonical Density Functional Theory. *J. Mater. Chem. A* **2020**, *8*, 20402−20407.
(48) Tang, Q.; Jiang, D. E. Mechanism of Hydrogen Evolution Reaction on 1T-MoS_2 from First Principles. *ACS Catal.* **2016**, *6*, 4953−4961.
(49) Liu, X.; Jiao, Y.; Zheng, Y.; Davey, K.; Qiao, S.-Z. A Computational Study on Pt and Ru Dimers Supported on Graphene for the Hydrogen Evolution Reaction: New Insight into the Alkaline Mechanism. *J. Mater. Chem. A* **2019**, *7*, 3648−3654.
(50) Légaré, M. A.; Bélanger-Chabot, G.; Dewhurst, R. D.; Welz, E.; Krummenacher, I.; Engels, B.; Braun-Schweig, H. Nitrogen Fixation and Reduction at Boron. *Science* **2018**, *359*, 896.
(51) Lindgren, P.; Kastlunger, G.; Peterson, A. A Challenge to the $\Delta G \sim 0$ Interpretation of Hydrogen Evolution. *ACS Catal.* **2020**, *10*, 121−128.
(52) Jain, A.; Bar Sadan, M.; Ramasubramaniam. Identifying a New Pathway for Nitrogen Reduction Reaction on Fe-Doped MoS_2 by the Coadsorption of Hydrogen and N_2. *J. Phys. Chem. C* **2021**, *125*, 19980−19990.
(53) Deng, J.; Li, H.; Wang, S.; Ding, D.; Chen, M.; Liu, C.; Tian, Z.; Novoselov, K. S.; Ma, C.; Deng, D.; Bao, X. Multiscale Structural and Electronic Control of Molybdenum Disulfide Foam for Highly Efficient Hydrogen Production. *Nat. Commun.* **2017**, *8*, 14430.
(54) Exner, K. S. Paradigm Change in Hydrogen Electrocatalysis: The Volcano's Apex is Located at Weak Bonding of the Reaction Intermediate. *Int. J. Hydrogen Energy* **2020**, *45*, 27221−27229.
(55) Nørskov, J. K.; Bligaard, T.; Logadottir, A.; Kitchin, J. R.; Chen, J. G.; Pandelov, S.; Stimming, U. Trends in the Exchange Current for Hydrogen Evolution. *J. Electrochem. Soc.* **2005**, *152*, J23.
(56) Ju, W.; Bagger, A.; Wang, X.; Tsai, Y.; Luo, F.; Möller, T.; Wang, H.; Rossmeisl, J.; Varela, A. S.; Strasser, P. Unraveling Mechanistic Reaction Pathways of the Electrochemical CO_2 Reduction on Fe-N-C Single-Site Catalysts. *ACS Energy Lett.* **2019**, *4*, 1663−1671.
(57) Huang, Q.; Liu, H.; An, W.; Wang, Y.; Feng, Y.; Men, Y. Synergy of a Metallic NiCo Dimer Anchored on a C_2N-Graphene Matrix Promotes the Electrochemical CO_2 Reduction Reaction. *ACS Sustain. Chem. Eng.* **2019**, *7*, 19113−19121.
(58) Yin, H.; Gan, L. Y.; Wang, P. The Identification of Optimal Active Boron Sites for N_2 Reduction. *J. Mater. Chem. A* **2020**, *8*, 3910−3917.
(59) Lei, Y.; Wang, Y.; Liu, Y.; Song, C.; Li, Q.; Wang, D.; Li, Y. Designing Atomic Active Centers for Hydrogen Evolution Electrocatalysts. *Angew. Chem., Int. Ed.* **2020**, *59*, 20794−20781.
(60) Choi, C.; Gu, G. H.; Noh, J.; Park, H. S.; Jung, Y. Understanding potential-dependent competition between electrocatalytic dinitrogen and proton reduction reactions. *Nat. Commun.* **2021**, *12*, 4353.
(61) Melander, M. M. Grand Canonical Rate Theory for Electrochemical and Electrocatalytic Systems I: General Formulation and Proton-coupled Electron Transfer Reactions. *J. El. Chem. Soc.* **2020**, *167*, 116518.
(62) Medford, A. J.; Wellendorff, J.; Vojvodic, A.; Studt, F.; Abild-Pedersen, F.; Jacobsen, K. W.; Bligaard, T.; Nørskov, J. K. Assessing the reliability of calculated ammonia synthesis rates. *Science* **2014**, *345*, 197−200.
(63) Ren, Y.; Yu, C.; Han, X.; Tan, X.; Wei, Q.; Li, W.; Han, Y.; Yang, L.; Qiu, J. Methanol-Mediated Electrosynthesis of Ammonia. *ACS Energy Lett.* **2021**, *6*, 3844−3850.
(64) Westhead, O.; Jervis, R.; Stephens, I. E. Is Lithium the Key for Nitrogen Electroreduction? *Science* **2021**, *372*, 1149−1150.
(65) Wang, T.; Zhang, Y.; Huang, B.; Cai, B.; Rao, R. R.; Giordano, L.; Sun, S.-G.; Shao-Horn, Y. Enhancing Oxygen Reduction Electrocatalysis by Tuning Interfacial Hydrogen Bonds. *Nat. Catal.* **2021**, *4*, 753−762.
(66) Wagner, A.; Sahm, C. D.; Reisner, E. Towards Molecular Understanding of Local Chemical Environment Effects in Electro- and Photocatalytic CO_2 Reduction. *Nat. Catal.* **2020**, *3*, 775−786.
(67) Wuttig, A.; Toste, F. D. The Interface is a Tunable Dimension in Electricity-Driven Organic Synthesis. *Nat. Sci.* **2021**, *1*, e20210036.
(68) Zhang, X.; Xue, D.; Jiang, S.; Xia, H.; Yang, Y.; Yan, W.; Hu, J.; Zhang, J. Rational Confinement Engineering of MOF-derived Carbon-based Electrocatalysts toward CO_2 Reduction and O_2 Reduction Reactions. *InfoMat* **2021**, DOI: 10.1002/inf2.12257.

https://doi.org/10.1021/acscatal.1c05820
ACS Catal. 2022, 12, 2505−2512